Circular dichroism and angular deviation in x-ray absorption spectra of $Dy_2ScN@C_{80}$ single-molecule magnets on *h*-BN/Rh(111)

T. Greber,[1] A. P. Seitsonen,[2] A. Hemmi,[1] J. Dreiser,[3] R. Stania,[1] F. Matsui,[4] M. Muntwiler,[3] A. A. Popov,[5] and R. Westerström[6]

[1]*Physik-Insitut, Universität Zürich, Winterthurerstrasse 190, CH-8057 Zürich, Switzerland*
[2]*Département de Chimie, École Normale Supérieure, 24 Rue Lhomond, F-75005 Paris, France*
[3]*Paul Scherrer Institut, CH-5232 Villigen, Switzerland*
[4]*Nara Institute of Science and Technology (NAIST), 8916-5 Takayama, Ikoma, Nara 630-0192, Japan*
[5]*Leibniz Institute of Solid State and Materials Research, Helmholtzstraße 20, D-01069 Dresden, Germany*
[6]*Division of Synchrotron Radiation Research, Lund University, SE-22100 Lund, Sweden*

(Received 22 October 2018; published 16 January 2019)

Endohedral fullerenes, such as $Dy_2ScN@C_{80}$, are single-molecule magnets with long relaxation times of their magnetization. An open and anisotropic $4f$ electron shell in the lanthanides (here Dy) imposes a magnetic moment that maintains its orientation at liquid-helium temperatures for macroscopic times. If these molecules shall be used as single-bit information storage elements or for quantum operations, the orientation of the endohedral units and the orientation of the magnetic moments has to be controlled. X-ray absorption spectroscopy (XAS) and magnetic circular dichroism (XMCD)—with variation of the angle of x-ray incidence—allows for the detection of these two structural elements. We present XMCD data of $Dy_2ScN@C_{80}$ on an *h*-BN/Rh(111) nanomesh that display at 2 K a large hysteresis with a coercive field of 0.4 T. The angular dependence of the XAS data at the Dy M_5 edge indicates partial ordering of the endohedral units. In order to quantify anisotropic orientation we introduce the "deviation" $\mathcal{D}$ as an operational quantity that measures differences between two spectra.

DOI: 10.1103/PhysRevMaterials.3.014409

I. INTRODUCTION

X-ray magnetic circular dichroism led to the discovery of single-molecule magnetism in endohedral fullerenes [1], and with x-ray angular dichroism it could be shown later that the endohedral cluster in $Dy_2ScN@C_{80}$ on a Rh surface orients preferentially in a fashion parallel to the surface [2]. Before presenting x-ray absorption data on $DySc_2N@C_{80}$ on *h*-BN/Rh(111) we briefly recall the physics of these $4f$-based endohedral single-molecule magnets (SMMs).

Immediately after the discovery of C_{60} [3], attempts to put host atoms or molecules inside these carbon cages were reported [4]. The understanding of the stability of this new form of carbon quickly progressed, where Hückel calculations for the empty fullerenes revealed the symmetries of closed shell or open shell icosahedral clusters such as C_{60} or C_{80} [5]. However, it took 15 more years until Stevenson *et al.* found a particularly stable form of C_{80} endofullerenes [6]. As predicted [7], C_{80} gets stable if the six-electron rule is obeyed, i.e., if six electrons are added into the highest occupied molecular orbital (HOMO) of C_{80}. These six electrons may stem from three trivalent 3^+ rare-earth ions and one central nitrogen 3^- ion that lead to the formation of a large HOMO-LUMO (lowest unoccupied molecular orbital) gap, as it is the case for empty C_{60}. Figure 1(a) shows a C_{80} molecule with an R_3N endohedral unit, where R is a positive trivalent rare-earth ion (cation) and N a negative nitrogen ion (anion). Figure 1(b) displays the Hückel energies of the 80 π orbitals of a C_{80} cage with icosahedral symmetry. The HOMO shell is eightfold degenerate, but there are only two electrons from the carbon cage left for filling this shell, which rationalizes the "six-electron rule." This six-electron rule for C_{80} may be satisfied as well by two trivalent rare-earth ions only if it is e.g. $La_2@C_{80}$ [8]. More interestingly, some rare-earth pairs trap an electron in the center of the molecule, while the missing electron in the carbon cage has to be provided by substitution of one carbon atom with nitrogen, or in adding an electron by an exohedral chemical bond [9].

The fact that also rare-earth ions with an open $4f$ shell may be packed into C_{80} [6] triggered the idea of using these molecules as fluorescence centers [10], or as single molecule magnets, which was addressed in $Tb_3N@C_{80}$ and $Ho_3N@C_{80}$ [11]. It took some more years until the first C_{80} single-molecule magnet $DySc_2N@C_{80}$ was discovered with the help of x-ray magnetic circular dichroism that relies on many orders of magnitude less material than is needed for state-of-the-art magnetometry with a superconducting quantum interference device (SQUID) [1]. The main physical reasons for the long-time stabilization of the magnetic moment of a single ion like Dy^{3+} lie in the Kramers symmetry of the $4f^9$ shell, the strong ligand field, mainly imposed by the central nitrogen ion, and the anisotropic charge distribution of the different J_z levels that form the $2J+1$ Hund manifold. Figure 2 shows the charge distribution of the $J_z = \pm 15/2$ states that turn out to be the ground states of $DySc_2N@C_{80}$. The charge distribution of these atomic states may be obtained analytically [12]. From Fig. 2 it becomes clear that an anisotropic charge distribution has a potential energy that depends on the orientation of the quantization axis with respect to the

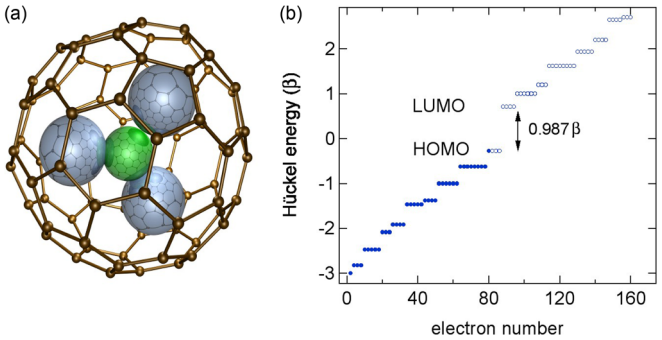

FIG. 1. (a) Model of $R_3N@C_{80}$, where the icosahedral isomer is shown. R blue, N green, and C brown. (b) Hückel eigenvalues of the 80 C p_z orbitals that are arranged in the icosahedral C_{80} geometry with a nearest-neighbor hopping parameter β. The HOMO-LUMO gap is 0.987β for C_{80}, as compared to 0.76β for C_{60}.

electrostatic field of the ligands. The excitation energy into the next higher states ($J_z = \pm 13/2$) is several $100k_B$ K, and thus the pseudospin model [13] that treats the magnetism with a pair of "spins" $\pm J_z$ is valid below 100 K. This furthermore means that we deal with noncollinear magnetism, i.e., that the magnetic moments do not freely follow the external magnetic field but remain aligned with respect to the Dy-N axes.

The interaction between different magnetic moments inside C_{80} turned out to be rather strong and decisive for the stability of the magnetization [13]. While we understand why $Dy_2ScN@C_{80}$ is the most stable single-molecule magnet in the $Dy_nSc_{3-n}N@C_{80}$, $n \in \{1, 2, 3\}$ series [13], the understanding of why the endohedral unit of $Dy_3N@C_{80}$ on Cu(111) [14], or $Dy_2ScN@C_{80}$ on Rh(111) [2], show a tendency to orient parallel to the surface, even at room temperature [14], was lacking. Likely, it is related to the nonisotropic electric field outside the C_{80} cage as it may be inferred from C 1s x-ray photoelectron spectroscopy (XPS) [15]. A second way to address the orientation of the endohedral unit is magnetic torque [16]. It is nevertheless a formidable task to tame the endohedral units, i.e., to control their orientation. In the following, we report on the endohedral orientation of $Dy_2ScN@C_{80}$ on an h-BN/Rh(111) nanomesh [17] as it is observed with x-ray absorption spectroscopy (XAS). We show

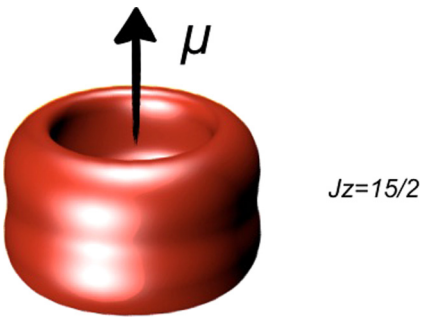

FIG. 2. Charge distribution in the $J_z = 15/2$ state of the Dy $4f^9$ shell as obtained using the formulas in Ref. [12]. The anisotropic shape implies an orientation in the ligand field. The magnetic moment μ of $10\mu_B$ points along the axis of the torus.

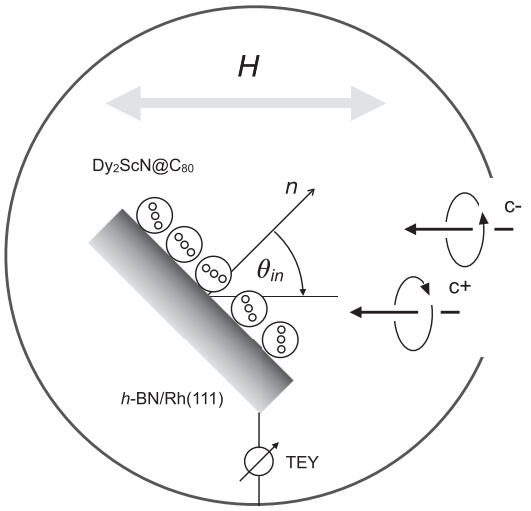

FIG. 3. Experimental setup of the x-ray absorption experiments at the X-Treme beamline. The total electron yield (TEY) of the emitted electrons upon absorption of circularly polarized x rays c^+ and c^- is measured. The external magnetic field H is parallel to the impinging x rays, while the x-ray incidence angle θ_{in} may be varied and is measured relative to the surface normal n. The sample, in the present case $Dy_2ScN@C_{80}$ on h-BN/Rh(111), may be cooled down to 2 K temperature and analyzed in externally applied fields $\mu_0 H$ between -7 and $+7$ T.

magnetic hysteresis and angular dependent x-ray absorption spectra. In order to access the differences in the absorption spectra we introduce the "deviation" $\mathcal{D}$ as an operational dimensionless quantity for measuring differences between two spectra recorded, e.g., at different x-ray incidence angles, where $\mathcal{D} > 0$ indicates angular dichroism.

II. EXPERIMENT

All x-ray absorption measurements have been performed at the X-Treme beam line of the Swiss Light Source [18] in the total electron yield mode with circularly polarized light. The x rays impinge parallel or antiparallel to the external magnetic field and the sample may be rotated away from normal incidence that is parallel to the applied field [2]. In Fig. 3 the experimental geometry of the x-ray absorption experiment where the circular polarization and the external magnetic field may be varied, and where the total electron yield (TEY) is measured, is shown. As a substrate we used h-BN/Rh(111) wafer samples that can be transported in air and cleaned by annealing according to Ref. [19]. The coverage was determined from a comparison of the nitrogen K edge x-ray absorption spectrum of one monolayer h-BN on Rh(111) with that of the Dy M_5 edge after adsorption and the corresponding x-ray absorption cross sections.

III. RESULTS AND DISCUSSION

The magnetism of the $4f$ shell was studied using x-ray magnetic circular dichroism (XMCD) at the Dy M_5 edge, where the difference in absorption between left and right

circularly polarized x-rays (c^- and c^+) is directly related to the magnetization of the endohedral Dy^{3+} ions. The element-specific magnetization curves were measured by recording the maximum XMCD signal while sweeping the magnetic field at a rate of 33 mT s^{-1} (for more details, see Ref. [2]). Figure 4 shows the magnetization curve of Dy from 1.3 monolayers (ML) $Dy_2ScN@C_{80}$ on an h-BN/Rh(111) nanomesh. Compared to $Dy_2ScN@C_{80}$ on Rh(111) [2] the hysteresis curve is more pronounced, which is ascribed to the better decoupling of the molecules from the metallic substrate by the h-BN layer. The concepts of "remanence" and "coercivity" are borrowed from hysteresis in ferromagnetic systems, though the finite lifetime of the magnetization in the SMMs calls for quoting the field scan rates and the photon flux, since x-ray absorption causes loss of magnetization [20]. For the parameters used in the XMCD experiments we find the largest coercivity of $\mu_0 H_c = 0.4$ T for 1.3-ML $Dy_2ScN@C_{80}$ on h-BN/Rh(111) as compared to 0.2 and <0.05 T for a multilayer and sub-ML of $Dy_2ScN@C_{80}$ on Rh(111), respectively [2], and ∼0.2 T for a self-assembled ML of functionalized $Dy_2ScN@C_{80}$ on Au(111) [21].

Compared to the hysteresis of $Dy_2ScN@C_{80}$ as measured with a SQUID of $H_c = 0.55$ T [13], the coercivity is similar and confirms the better decoupling between the Rh and the Dy of the single-layer h-BN.

Now we turn to the analysis of endohedral ordering with the help of the variation of the x-ray absorption spectra as a function of the x-ray incidence angle. At sufficiently low temperatures all conformational degrees of freedom are frozen. If the degeneracy of the $4f$ Hund manifold is lifted, and if there is a preferential orientation of the Dy-N axes, the x-ray absorption spectra depend on the angle between the magnetic moment and the x-ray incidence direction. In Ref. [2] such angular dichroism was shown in comparing the total electron yield of the two x-ray helicities in an applied magnetic field, as well as the sum of the spectra of left I_L and right I_R circularly polarized light for different x-ray incidence angles. If $I_L + I_R$ is considered to represent linear polarized x-ray absorption, this is as well a form of x-ray linear dichroism XLD. While standard XLD is the x-ray absorption difference of two orthogonal linear polarizations $I_H - I_V$, the sum of circular polarized light $I_L + I_R$ defines the plane spanned by the vectors H and V only. In order to get structural information such as the orientation of the Dy-N axes, we need an angular dependence that is obtained in the case of circular dichroism by rotating the x-ray incidence with respect to the surface normal [2]. Since the transmission of the total electron yield in our instrument may depend on the applied field and the emission angle, we have to normalize the spectra and thus use the deviation $\mathcal{D}$ for an expression of the angular dichroism. $\mathcal{D}$ is defined as the integral of the absolute value of

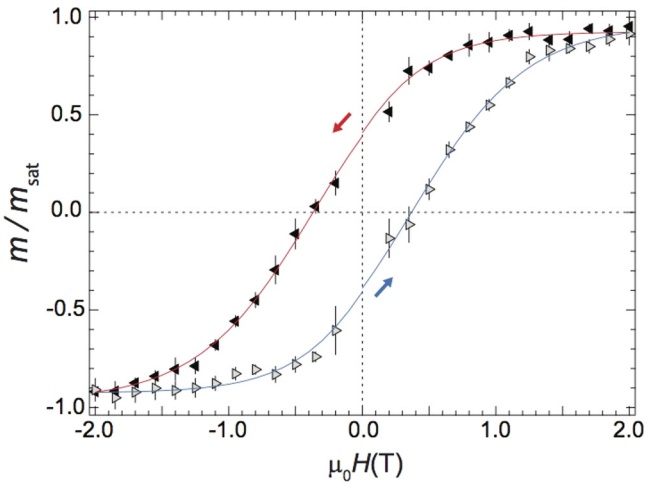

FIG. 4. X-ray magnetic circular dichroism (XMCD) m of the hysteresis of 1.3 monolayers of $Dy_2ScN@C_{80}$ on h-BN/Rh(111), at the photon energy in the Dy M_5 edge with maximum dichroism. The dichroism is normalized with the saturation value m_{sat} at 6.5 T. The temperature was set to 2 K, the field scan rate was 33 mT s^{-1}, normal photon incidence $\theta_{in} = 0°$, and the photon flux 2.5×10^{10} ph mm^{-2} s^{-1}. The magnetization curve corresponds to the average of several independent measurements, where the error bars are the standard deviation at each magnetic field setting. The arrows indicate the ramping direction of the magnetic field, and the lines are guides to the eye.

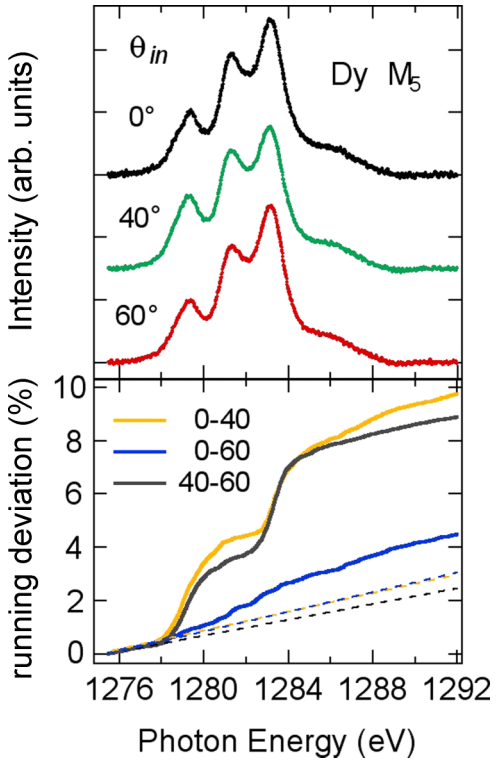

FIG. 5. Top panel: Dy M_5 edge x-ray absorption spectra of $Dy_2ScN@C_{80}$ on h-BN/Rh(111) for different incidence angles θ_{in} of the radiation measured with respect to the surface normal. The spectra are the sum of the two helicities (c^+ and c^-) and are recorded at a temperature set to 2 K in a field of 6.5 T parallel to the photon incidence. The $4f^{10}3d^9$ final state multiplet appears to depend on the photon incidence angle θ_{in}, which can be explained with endohedral orientation with respect to the surface. The bottom panel shows the running deviation [with $E_0 = 1275$ eV, see Eq. (1)] of the three spectra in the top panel and the corresponding statistical noise (dashed lines). The deviation between the spectrum at normal incidence and 40° incidence (yellow) is largest, while the spectrum at 60° resembles that of normal incidence (blue).

TABLE I. Deviations $\mathcal{D}$ of different Dy M_5 XAS spectra of left and right polarized x rays of $Dy_2ScN@C_{80}$ after background subtraction for three different x-ray incidence angles θ_{in} recorded at a temperature set to 2 K and a field of 6.5 T. The background is inferred from the slope in the running deviation before and after the XAS peak.

Substrate	θ_{in}^A, θ_{in}^B (deg)	$\mathcal{D}$ (%)	Reference
Rh(111)	0, 45	7.8	[2]
submonolayer	0, 60	11.7	[2]
	45, 60	3.3	[2]
h-BN/Rh(111)	0, 40	6.8	This work
1.3 ML	0, 60	1.4	This work
	40, 60	6.4	This work

the difference of two background subtracted and normalized spectra A and B [$\int I_A(E)dE = \int I_B(E)dE = 1$] that shall be compared,

$$\mathcal{D}_{A,B} = \int_{E_0}^{E_1} |(I_A - I_B)|dE, \tag{1}$$

where the energy interval of interest lies between E_0 and E_1. The deviation $\mathcal{D}$ is a bound, dimensionless quantity or number $0 \geqslant \mathcal{D} \geqslant 2$, where $\mathcal{D} = 0$ indicates identical spectra and $\mathcal{D} = 2$ disjunct spectra without an overlap. As we can see in the bottom panel of Fig. 5, the noise also contributes to the deviation but can be quantified and subtracted for meaningful comparisons.

The deviation may as well be calculated for theoretical spectra, where it is possible to extract the maximum deviation that can be expected for perfectly ordered $DySc_2N@C_{80}$ species, where the x rays impinge perpendicular ($\perp$) to the endohedral plane that is spanned by the three rare-earth ions (A) or parallel ($\parallel$) to the Dy-N axis (B) [2]. For the case of the Dy M_5 edge we get a $\mathcal{D}_{\perp,\parallel}$ of 32%, which is an upper bound for the expected deviations of the experimental data. The three measured deviations of $Dy_2ScN@C_{80}$ on *h*-BN/Rh(111) indicate endohedral ordering. In comparing them with the corresponding ones of $Dy_2ScN@C_{80}$ on Rh(111) (Table I), we see that the *h*-BN/Rh(111) substrate imposes less anisotropy than the bare Rh(111), where it was found that the endohedral units of molecules in the first layer orient parallel to the substrate [2]. However, the fact that for *h*-BN/Rh(111) the spectrum at $\theta_{in} = 40^\circ$ is significantly different from that at $\theta_{in} = 0^\circ$ or $\theta_{in} = 60^\circ$, and that the deviation between $\theta_{in} = 0^\circ$ and $\theta_{in} = 60^\circ$ is very small, shows that the endohedral ordering is not as simple as in the case of $Dy_2ScN@C_{80}$/Rh(111), since this $\mathcal{D}$ behavior must involve different endohedral orientations.

IV. CONCLUSION

In conclusion, we have shown that monolayer quantities of endohedral single-molecule magnets on an *h*-BN/Rh(111) nanomesh display large coercive fields, close to the value of bulk samples. Compared to a bare Rh(111) substrate, the additional *h*-BN spacer layer imposes larger hysteresis loops. On the other hand, the spacer layer imposes less ordering of the endohedral units as it is inferred from the introduced angular deviation $\mathcal{D}$. This order parameter is important information if the $4f$ electron-derived single-ion magnets shall be "tamed" and arranged on a surface in a controlled way.

ACKNOWLEDGMENTS

The x-ray circular magnetic dichroism and absorption spectroscopy data were recorded at the X-Treme beam line at the Swiss Light Source in Villigen. We gratefully acknowledge financial support from the Swiss National Science Foundation (SNF Projects No. 200021, No. 129861, No. 147143, and No. PZ00P2-142474), the Deutsche Forschungsgemeinschaft (DFG Project No. PO 1602/1-1), the Swedish Research Council (Grant No. 2015-00455), the Sklodowska Curie Actions cofounding project INCA 600398, and the European Research Council (ERC) under the European Union Horizon 2020 research and innovation programme (Grant Agreement No. 648295 GraM3) (to A.A.P.).

[1] R. Westerström, J. Dreiser, C. Piamonteze, M. Muntwiler, S. Weyeneth, H. Brune, S. Rusponi, F. Nolting, A. Popov, S. Yang *et al.*, J. Am. Chem. Soc. **134**, 9840 (2012).

[2] R. Westerström, A.-C. Uldry, R. Stania, J. Dreiser, C. Piamonteze, M. Muntwiler, F. Matsui, S. Rusponi, H. Brune, S. Yang *et al.*, Phys. Rev. Lett. **114**, 087201 (2015).

[3] H. Kroto, J. Heath, S. OBrien, R. Curl, and R. Smalley, Nature (London) **318**, 162 (1985).

[4] J. Heath, S. O'Brien, Q. Zhang, Y. Liu, R. Curl, H. Kroto, F. Tittel, and R. Smalley, J. Am. Chem. Soc. **107**, 7779 (1985).

[5] P. Fowler, Chem. Phys. Lett. **131**, 444 (1986).

[6] S. Stevenson, G. Rice, T. Glass, K. Harich, F. Cromer, M. Jordan, J. Craft, E. Hadju, R. Bible, M. Olmstead *et al.*, Nature (London) **402**, 898 (1999).

[7] K. Nakao, N. Kurita, and M. Fujita, Phys. Rev. B **49**, 11415 (1994).

[8] T. Kato, J. Mol. Struct. **838**, 84 (2007).

[9] F. Liu, D. S. Krylov, L. Spree, S. M. Avdoshenko, N. A. Samoylova, M. Rosenkranz, A. Kostanyan, T. Greber, A. U. B. Wolter, B. Büchner *et al.*, Nat. Commun. **8**, 16098 (2017).

[10] R. Macfarlane, D. Bethune, S. Stevenson, and H. Dorn, Chem. Phys. Lett. **343**, 229 (2001).

[11] M. Wolf, K.-H. Müller, D. Eckert, Y. Skourski, P. Georgi, R. Marczak, M. Krause, and L. Dunsch, J. Magn. Magn. Mater. **290**, 290 (2005).

[12] J. Sievers, Z. Phys. B **45**, 289 (1982).

[13] R. Westerström, J. Dreiser, C. Piamonteze, M. Muntwiler, S. Weyeneth, K. Kraemer, S.-X. Liu, S. Decurtins, A. Popov, S. Yang *et al.*, Phys. Rev. B **89**, 060406(R) (2014).

[14] M. Treier, P. Ruffieux, R. Fasel, F. Nolting, S. Yang, L. Dunsch, and T. Greber, Phys. Rev. B **80**, 081403(R) (2009).

[15] R. Stania, A. P. Seitsonen, D. Kunhardt, B. Buechner, A. A. Popov, M. Muntwiler, and T. Greber, J. Phys. Chem. Lett. **9**, 3586 (2018).

[16] A. Kostanyan, R. Westerström, Y. Zhang, D. Kunhardt, R. Stania, B. Buechner, A. A. Popov, and T. Greber, Phys. Rev. Lett. **119**, 237202 (2017).

[17] M. Corso, W. Auwärter, M. Muntwiler, A. Tamai, T. Greber, and J. Osterwalder, Science **303**, 217 (2004).

[18] C. Piamonteze, U. Flechsig, S. Rusponi, J. Dreiser, J. Heidler, M. Schmidt, R. Wetter, M. Calvi, T. Schmidt, H. Pruchova *et al.*, J. Synchrotron Radiat. **19**, 661 (2012).

[19] A. Hemmi, C. Bernard, H. Cun, S. Roth, M. Klöckner, T. Kälin, M. Weinl, S. Gsell, M. Schreck, J. Osterwalder *et al.*, Rev. Sci. Instrum. **85**, 035101 (2014).

[20] J. Dreiser, R. Westerström, C. Piamonteze, F. Nolting, S. Rusponi, H. Brune, S. Yang, A. Popov, L. Dunsch, and T. Greber, Appl. Phys. Lett. **105**, 032411 (2014).

[21] C. H. Chen, D. S. Krylov, S. M. Avdoshenko, F. Liu, L. Spree, R. Westerström, C. Bulbucan, M. Studniarek, J. Dreiser, A. U. B. Wolter *et al.*, Nanoscale **10**, 11287 (2018).